

Spatial-Temporal Multi-Scale Quantization for Flexible Motion Generation

Zan Wang^{1,2*}, Jingze Zhang^{2,3*}, Yixin Chen², Baoxiong Jia², Wei Liang^{1,4†}, Siyuan Huang^{2†}

* indicates equal contribution † indicates corresponding authors

¹ School of Computer Science & Technology, Beijing Institute of Technology

² State Key Laboratory of General Artificial Intelligence, BIGAI

³ Department of Automation, Tsinghua University

⁴ Yangtze Delta Region Academy of Beijing Institute of Technology, Jiaxing

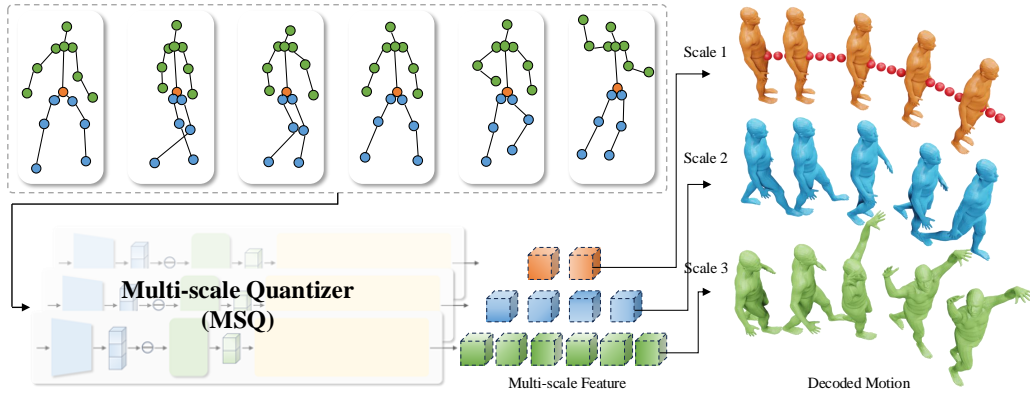


Figure 1: We propose MSQ, a novel quantization method that compresses human motion into a multi-scale discrete token space across temporal and spatial dimensions, facilitating the effectiveness and flexibility in diverse motion modeling tasks. Each scale captures different granularities of motion features, resulting in distinct motion sequences upon decoding. Our project website is available at <https://sites.google.com/view/msquantizer>.

Abstract

Despite significant advancements in human motion generation, current motion representations—typically formulated as discrete frame sequences—still face two critical limitations: (i) they fail to capture motion from a multi-scale perspective, limiting the capability in complex patterns modeling; (ii) they lack compositional flexibility, which is crucial for model’s generalization in diverse generation tasks. To address these challenges, we introduce MSQ, a novel quantization method that **compresses the motion sequence into multi-scale discrete tokens across spatial and temporal dimensions**. MSQ employs distinct encoders to capture body parts at varying spatial granularities and temporally interpolates the encoded features into multiple scales before quantizing them into discrete tokens. Building on this representation, we establish a generative mask modeling model to effectively support motion editing, motion control, and conditional motion generation. Through quantitative and qualitative analysis, we show that our quantization method enables the seamless composition of motion tokens without requiring specialized design or re-training. Furthermore, extensive evaluations demonstrate that our approach outperforms existing baseline methods on various benchmarks.

1 Introduction

Human motion generation [46, 22, 47, 57, 70, 36, 29, 23] has progressed significantly in the past few years, driving various applications in fields like virtual reality, video games, and film production. Recent advancements have also pivoted towards practical objectives such as motion editing [72, Preprint. Under review.

5, 19] and motion control [32, 53, 64], empowering creators to customize motion outputs to their specific requirements. Supporting these diverse tasks requires a comprehensive and flexible motion representation—a long-standing goal pursued by the community for years.

Current methods [7, 22, 36, 61, 25, 17] predominantly rely on skeleton-based representations, where human motion is defined as a sequence of single-frame body poses, modeled by joint positions or statistical parametric models like SMPL [40]. Some approaches [70, 41, 10, 13] further compress these data into continuous or discrete latent spaces via Variational Autoencoder (VAE) [34] or VQ-VAE [59] to facilitate the learning process of generative models. Despite progress, these representations still encounter two fundamental limitations, failing to capture the complex dynamics necessary for effective and flexible motion modeling.

First, current motion representations lack multi-scale modeling across both temporal and spatial dimensions. Multi-scale modeling, interpreting data at multiple levels, has proven essential in capturing complex patterns for image modeling [39, 30, 58]. In the context of human motion, multi-scale modeling enables models to capture high-level semantic patterns and fine-grained dynamic details over time. Spatially, it distinguishes coarse motion trajectories from individual joint movements, offering a more nuanced understanding of motion structure.

Second, existing methods struggle to handle compound motions due to insufficient compositional capacity. A representation with a robust compositional structure would enable generative models to generalize to unseen motion compositions, significantly enhancing the flexibility and precision of diverse fine-grained motion editing and part-based motion control tasks. Though recent approaches [49, 76, 60] decompose the whole body into parts for feature learning in the latent space, they remain intractable when directly composing different motion components.

To address these issues, *we introduce a novel motion quantization method, denoted as MSQ, which compresses motion sequences into multi-scale discrete tokens across spatial and temporal dimensions*, as illustrated in Fig. 1. Once encoding the motion into discrete tokens, we model the motion distribution through a generative masked Transformer [8, 23, 50], enabling diverse applications in motion editing, motion control, and conditional motion generation. Specifically, MSQ uses separate CNN-based encoders to capture decomposed body parts at varying spatial granularities, followed by corresponding interpolation operations at different temporal scales. This technique depicts the coarse motion features like the pelvis trajectories at a higher level with fewer tokens, while finer features like limb dynamics are the opposite. Rather than relying on conventional vector quantization [70, 23], we adopt Finite Scalar Quantization (FSQ) [43] to quantize latent features into discrete token indices, mitigating the code index collapse during training. For reconstruction, MSQ merges the dequantized codes and projects them back into the original motion space via a single decoder network.

Through quantitative and qualitative analysis, we showcase how the feature at each scale contributes to the motion representation and how MSQ supports the seamless composition of motion tokens, which enables versatile motion editing and control tasks without requiring model modifications or fine-tuning. We also conduct extensive experiments across diverse benchmarks to demonstrate our method’s superiority. Our method outperforms the state-of-the-art text-based motion editing methods on the MotionFix [5]. For conditional motion generation, our method achieves superior performance on the HumanML3D [22] and significantly enhances language-guided human-scene interaction (HSI) generation on the HUMANISE [61].

Our contributions are summarized as follows: (1) We propose a novel motion quantization method that compresses motion sequences into a multi-scale discrete token space, integrating generative masked modeling to support diverse motion modeling tasks. (2) We analyze the impact of each scale within the proposed multi-scale representation and showcase its inherent capacity for seamless motion composition, which enables flexible motion editing and control. (3) Extensive evaluations demonstrate our method’s superiority over existing methods on various benchmarks, including MotionFix, HumanML3D, and HUMANISE.

2 Related Work

Human Motion Generation Early work on human motion generation primarily focused on motion forecasting given historical motion sequences [42, 68, 7]. Leveraging annotated motion data, several studies [3, 21, 46, 47, 22, 71, 57, 70, 10, 50] introduced methods to generate diverse and realistic

human motions conditioned on semantic cues like action labels and text descriptions. Recently, efforts have extended to other conditional modalities, such as audio [69, 11], object [74, 36, 28, 17], 3D scenes [4, 66, 29, 62], and interactive movements [38, 65], further booming motion generation research. These approaches often model motion probability distributions using generative models like diffusion models [57, 10, 25]. Another direction [45, 63, 12] formulates motion generation as a Markov Decision Process (MDP), applying Reinforcement Learning (RL) to learn policies for avatar movement control. Besides conditional motion generation, motion editing has been a long-standing focus, including style transfer [1, 26, 55] and recent text-guided editing of specific body parts [72, 19, 5]. With diffusion models, some methods [32, 53, 64] incorporate spatial guidance (*e.g.*, trajectories and joint positions) into the denoising process to enable control over motion generation. We introduce a multi-scale motion representation to support diverse motion generation tasks with enhanced effectiveness and flexibility. Besides, the inherent composition capability allows the seamless composition of motion tokens without requiring model modifications or re-training.

Motion Representation Modeling Most works [68, 7, 22, 36] represent motion as a sequence of joint positions or rotations, often called a skeleton-based representation. Some methods [42, 75] transform this spatial-temporal data into the frequency domain using discrete cosine transform (DCT) [2] to improve learning efficiency. Other methods [46, 61, 25, 17] leverage statistical parametric models like SMPL(-X) [40, 44], which capture body translation, orientation, pose, and shape. Rempe et al. [52], Zhang et al. [73] learn motion prior from existing datasets, often serving as regularization terms to further enhance motion modeling. To enable auto-regressive modeling, Zhang et al. [70], Lu et al. [41] quantize motion frames into discrete tokens using VQ-VAE; in contrast, Chen et al. [10], Dai et al. [13] employ a VAE to compress motion into a latent space, followed by a latent diffusion model for generation. Recent methods [49, 76, 60, 56] decompose the body into separate parts to achieve expressive features for motion generation and control. Pi et al. [49], Wan et al. [60] quantize per-frame body parts into discrete tokens; however, they neglect the multi-scale properties inherent in the motion data, reducing the modeling capability and flexibility. Unlike these works, our approach models motion in a discrete latent space with multi-scale features across spatial and temporal dimensions, possessing improved effectiveness and flexibility for various motion modeling tasks.

Generative Modeling Over the past decades, the computer vision community has explored various generative models for image generation, starting with Generative Adversarial Networks (GAN) [20, 31] and progressing to diffusion models [24, 15, 54], which now dominate the field. Recently, auto-regressive models [18, 67, 58] and generative masked modeling [14, 8, 9, 37] have also gained significant attention for their high-quality generation capabilities. The motion generation field has followed a similar developmental trajectory in many ways. Early methods [46, 47, 61] primarily rely on conditional Variational Autoencoder (cVAE) for generating motion conditioned on inputs like text descriptions, especially when the dataset scale is limited. MDM [57] is the first to introduce diffusion models into human motion generation, inspiring a wave of follow-up research [10, 25, 13]. Some approaches [70, 41, 27] represent motion frames as discrete tokens and use decoder-only transformers to generate motion auto-regressively. More recently, generative masked modeling [23, 50] has demonstrated notable improvements over diffusion and auto-regressive models, paving the way for new advancements in the field. This work integrates the proposed multi-scale quantization with generative masked modeling, achieving improved performance on diverse benchmarks [5, 22, 61].

3 Preliminaries

Finite Scalar Quantization (FSQ) FSQ [43], as a drop-in replacement for vector quantization, avoids issues like codebook collapse and the need for complex mechanisms like commitment losses [59] and code reinitialization [16]. Given a vector $z \in \mathbb{R}^d$, FSQ maps each entry z_i to a discrete space with L values through a bounding function $f : z \mapsto \lfloor L/2 \rfloor \tanh(z)$ followed by a rounding operation, finally yielding a quantized vector $\hat{z} = \text{round}(f(z))$. Assuming the i -th channel is mapped to L_i values, FSQ ultimately results in an implied codebook \mathcal{C} with size $|\mathcal{C}| = \prod_{i=1}^d L_i$. Additionally, FSQ employ straight-through estimator (STE) [6] to propagate gradients through the round operation by applying the stop-gradient mechanism, *i.e.*, $\text{round_ste} : z \mapsto z + \text{sg}(\text{round}(f(z)) - z)$. For more details, we recommend referring to the original paper.

Masked Transformer Generative masked modeling [14, 8, 9, 37] is a self-supervised learning technique where a model learns to predict a set of random masked tokens based on the known tokens. Recent approaches [8, 23, 50] have employed this learning paradigm to train bidirectional masked

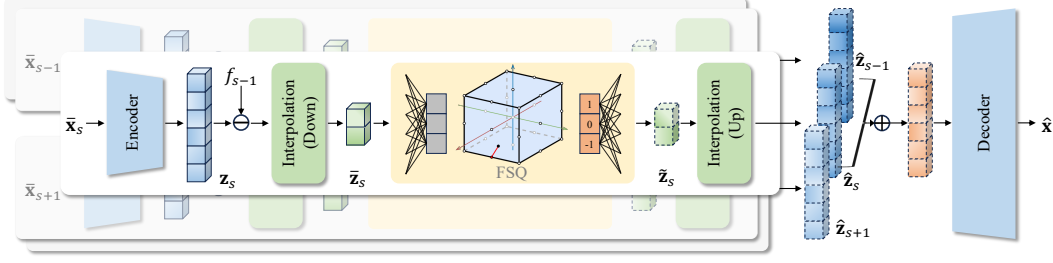


Figure 2: **Overview of MSQ.** MSQ separately compresses motion features at various spatial and temporal granularities, producing a multi-scale discrete token representation. These dequantized features are merged and passed to a decoder for motion reconstruction.

transformers for content generation in an auto-regressive manner. Specifically, during training, a random subset of content tokens is sampled and replaced with the special [MASK] token, with the masking ratio drawn from a pre-defined scheduling function $\gamma(r) \in (0, 1]$, where r is uniformly sampled. The masked transformer then learns to reconstruct the masked tokens from the observed ones. During sampling, the model begins with a fully masked token sequence and generates all tokens auto-regressively in two steps: (1) It generates a complete token sequence using the masked transformer. (2) It re-masks $\lceil \gamma(k/K) \cdot n \rceil$ tokens with the lowest confidence while maintaining the other tokens unchanged for subsequent iterations. n is the number of content tokens, and k is the current iteration step. This sampling process continues for K iterations.

4 Method

We propose a novel motion quantization method, *i.e.*, MSQ, which encodes human motion into multi-scale discrete tokens across spatial and temporal dimensions. Fig. 2 illustrates the design of MSQ. Building on this multi-scale representation, we develop a masked transformer to support diverse motion modeling tasks. Below, we provide a detailed description of each component.

4.1 Spatial-Temporal Multi-Scale Quantization

Given a human motion sequence $\mathbf{x} \in \mathbb{R}^{N \times D}$, where N is the number of motion frames and D is the dimensionality of each frame’s pose representation, MSQ aims to compress \mathbf{x} into a discrete token sequence \mathbf{y} with a multi-scale structure.

Encoding To achieve a multi-scale representation, MSQ first follows prior works [49, 60] to decompose \mathbf{x} into S sub-features, denoted as $\{\bar{\mathbf{x}}_s\}_{s=1}^S$. Each sub-feature $\bar{\mathbf{x}}_s \in \mathbb{R}^{N \times D_s}$ captures motion features related to specific body parts. Here, $D_s \leq D_{s+1}$ allows each feature $\bar{\mathbf{x}}_s$ to represent an increasingly finer granularity of motion, with coarser scales capturing coarse motion trends and finer scales retaining detailed motion nuances. For instance, the coarsest scale feature $\bar{\mathbf{x}}_1$ captures the motion trajectory through the pelvis joint, providing a rough depiction of motion; full-body features are retained at the finest scale (*i.e.*, $s = S$), ensuring precise representation of detailed motion. We then encode $\bar{\mathbf{x}}_s$ into a latent representation $\mathbf{z}_s \in \mathbb{R}^{n_s \times d}$ using a unique convolutional encoder per scale, following Pi et al. [49], Wan et al. [60]. Here, n/N is the down-sampling factor, and d represents the dimensionality of the latent space.

Next, we interpolate \mathbf{z}_s along the temporal dimension to produce vector $\bar{\mathbf{z}}_s = \text{Inter}(\mathbf{z}_s)$, where $\bar{\mathbf{z}}_s \in \mathbb{R}^{n_s \times d}$ and $\text{Inter}(\cdot)$ is the interpolation operation, yielding a sequence of multi-scale latent feature $\{\bar{\mathbf{z}}_s\}_{s=1}^S$. By setting $n_s \leq n_{s+1}$, we ensure that fewer tokens represent high-level motion information while progressively more tokens for low-level details, enhancing the expressiveness of the representation.

Quantization We apply FSQ [43] to quantize each latent vector $\bar{\mathbf{z}}_s$, yielding a quantized vector $\tilde{\mathbf{z}}_s = \text{FSQ}(\bar{\mathbf{z}}_s)$, where $\tilde{\mathbf{z}}_s \in \mathbb{R}^{n_s \times d}$. Each quantized vector $\tilde{\mathbf{z}}_s$ corresponds to a discrete index sequence $\mathbf{y}_s \in \{1, \dots, |\mathcal{C}|\}^{n_s}$. We concatenate index sequences of all scales (*i.e.*, $\{\mathbf{y}_s\}_{s=1}^S$) to form the final index sequence \mathbf{y} .

Decoding To reconstruct the original motion sequence, we begin by interpolating each quantized code $\tilde{\mathbf{z}}_s$ back to $\hat{\mathbf{z}}_s \in \mathbb{R}^{n_s \times d}$. Next, we merge the codes $\{\hat{\mathbf{z}}_s\}_{s=1}^S$ and forward the result through a

decoder implemented with de-convolution layers to produce the reconstructed motion $\hat{\mathbf{x}}$. Inspired by Lee et al. [35], we improve learning efficiency by interpolating and quantizing the residual features instead of directly quantizing $\bar{\mathbf{z}}_s$ in the implementation. Specifically, we apply $\bar{\mathbf{z}}_s = \text{FSQ}(\text{Inter}(\mathbf{z}_s - f_{s-1}))$ and define $f_s = \sum_{i=1}^s \bar{\mathbf{z}}_i$. This approach allows us to aggregate the dequantized residual features $\bar{\mathbf{z}}_s$ across all scales through simple addition. We pass the final aggregated result f_S to the decoder for motion reconstruction.

Training Objective We train MSQ end-to-end using the following loss function:

$$\mathcal{L} = \|\mathbf{x} - \hat{\mathbf{x}}\| + \alpha \sum_{s=1}^S (\|\mathbf{z}_s - \text{sg}(f_s)\| + \|\text{sg}(\mathbf{z}_s) - f_s\|). \quad (1)$$

Here, $\text{sg}(\cdot)$ denotes the stop gradient, and $\alpha = 0.1$ specifies the loss weight. While FSQ [43] removes the need for VQ objective and commitment loss terms, we retain them to accelerate convergence.

4.2 Mask Modeling for Diverse Tasks

Building on MSQ, we incorporate generative masked modeling to support diverse motion generation tasks by training a bidirectional masked transformer, as shown in Fig. 3. Specifically, after quantizing motions from the dataset into discrete tokens, the model learns to generate motion tokens with or without other conditions by modeling the tokens’ distribution in an auto-regressive manner. The training objective is to minimize the negative log-likelihood of the target token predictions. Below, we describe the model’s task-specific adaptations in detail.

Motion Composition MSQ inherently supports flexible motion composition by directly combining tokens from different motion sequences, as shown in Fig. 3a. For instance, given two motion sequences, \mathbf{x}^1 and \mathbf{x}^2 , we quantize them into token sets $\{\mathbf{y}_s^1\}_s^S$ and $\{\mathbf{y}_s^2\}_s^S$. To create a composite sequence, we concatenate tokens as $\{[\mathbf{y}_{s,1:i}^1; \mathbf{y}_{s,i+1:n_s}^2]\}_{s=1}^S$, enabling motion blending along the temporal dimension, as the token order corresponds to temporal progression. We then decode the composed tokens to a motion sequence that resembles \mathbf{x}^1 in the initial frames and transitions to resemble \mathbf{x}^2 in the subsequent frames. For spatial composition, we similarly combine tokens across different scales, $[\mathbf{y}_{1:s}^1; \mathbf{y}_{s+1:S}^2]$. This composition results in a motion that captures \mathbf{x}^1 partial parts’ dynamics, primarily represented by scales 1 to s with residual modeling, while the remaining parts resemble \mathbf{x}^2 .

Motion Control Once MSQ and the masked transformer are trained, our method enables motion control generation by providing a pelvis trajectory without requiring model modification or re-training. Specifically, we directly quantize the concatenation of pelvis trajectory and zero paddings into discrete tokens. By taking the first scale tokens corresponding to the pelvis and other scales’ masked tokens, the pre-trained masked transformer recovers the masked tokens, resulting in a motion sequence that aligns well with the specified trajectory, as illustrated in Fig. 3b.

Text-based Motion Editing For text-based motion editing (*i.e.*, the MotionFix [5] setting), we use MSQ to quantize both source and target motions into discrete tokens. Given the editing text and source motion tokens \mathbf{y}^{src} as input, we train the transformer to predict the target tokens \mathbf{y}^{tar} in a *single* iteration. As shown in Fig. 3c, we can optionally mask the editing part of the source tokens.

Conditional Motion Generation For conditional motion generation in Fig. 3d, we directly concatenate the conditional token embeddings (*e.g.*, derived from CLIP [51] for text-to-motion task) with the fully masked motion tokens. This concatenation is then passed through the masked transformer to predict the ground truth tokens in K iterations.

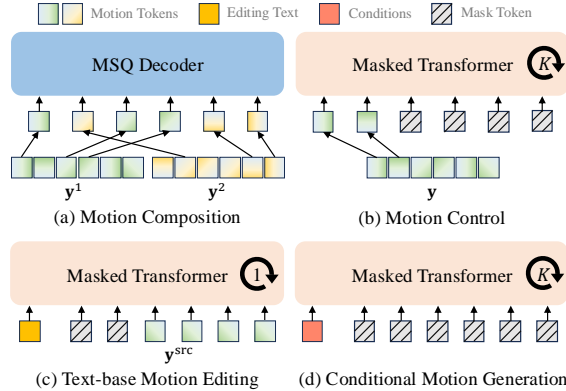


Figure 3: **Task-specific adaptations of our model for diverse tasks.** The light green and yellow colors indicate that the tokens are derived from two different motions.

Table 1: The scale impact on reconstruction quality.

Model	R-Precision (Top 1) \uparrow	FID \downarrow	MM Dist. \downarrow	MPJPE \downarrow
Real	0.511 \pm .003	0.002 \pm .000	2.974 \pm .008	0.0 \pm .000
MSQ (1,1)	0.279 \pm .003	5.781 \pm .031	4.589 \pm .011	108.63 \pm .083
MSQ (1,2)	0.323 \pm .005	5.554 \pm .017	4.413 \pm .017	87.88 \pm .130
MSQ (1,3)	0.378 \pm .000	5.285 \pm .016	4.021 \pm .014	68.10 \pm .055
MSQ (1,4)	0.494 \pm .000	0.158 \pm .002	3.042 \pm .036	44.60 \pm .034
MSQ (1,5)	0.505 \pm .000	0.077 \pm .001	2.966 \pm .011	34.41 \pm .036
w/o MSQ (1)	0.446 \pm .000	1.060 \pm .005	3.286 \pm .012	68.98 \pm .138
w/o MSQ (2)	0.483 \pm .000	0.296 \pm .003	3.051 \pm .012	50.67 \pm .078
w/o MSQ (3)	0.472 \pm .004	0.509 \pm .003	3.209 \pm .010	49.69 \pm .042
w/o MSQ (4)	0.478 \pm .003	0.347 \pm .002	3.053 \pm .010	43.10 \pm .043
w/o MSQ (5)	0.501 \pm .004	0.093 \pm .001	2.984 \pm .011	36.63 \pm .040
w/o MSQ (6)	0.505 \pm .000	0.077 \pm .001	2.966 \pm .011	34.41 \pm .036
Full Model	0.511 \pm .000	0.037 \pm .000	2.934 \pm .012	23.67 \pm .050

4.3 Implementation

We train both MSQ and the masked transformer using a CosineAnnealingWarmup scheduler [33] with a maximum learning rate of 10^{-4} and a minimum of 10^{-5} , alongside the Adam optimizer. MSQ is trained on 2 Nvidia RTX 3090 GPUs with a batch size of 128 per GPU, while the masked transformer is trained on 4 Nvidia RTX 3090 GPUs with a batch size of 16 per GPU. To schedule the training of the masked transformer, we follow prior works [8, 23] to adopt a cosine function $\gamma(\cdot)$. By default, we fix $S = 6$ in MSQ and $K = 5$ during the sampling.

5 Experiments

This section begins with a comprehensive analysis of the proposed multi-scale motion representation, followed by extensive quantitative and qualitative evaluations across a range of benchmarks.

5.1 Analysis of Multi-Scale Representation

To analyze the capability of MSQ, we adopt the HumanML3D [22] as the training data source. Details about the dataset and evaluation metrics are illustrated in Sec. 5.3.

Impact of Per Scale on Reconstruction We analyze the impact of each scale in our multi-scale representation through two ablative validations: (1) evaluating the contribution of the first s scales to motion reconstruction by merging and decoding tokens only from these scales, denoted as “MSQ (1, s)”; (2) assessing the effect of each individual scale on the final reconstruction by removing the tokens at that scale, denoted as “w/o MSQ (s)”.

The quantitative results are presented in Tab. 1. The results show that reconstruction performance improves as the number of scales used for decoding increases. Notably, metrics like *FID* show a sudden increase when the fourth scale works. **We speculate that this scale incorporates features of the arms, whose dynamic richness significantly contributes to these metrics.** Ablation studies for individual scales also reveal that the first scale, which primarily encodes pelvis information, is the most critical, with the impact of subsequent scales gradually diminishing.

We visualize the reconstruction results of “MSQ (1, s)” in Fig. 4. From the visualizations, we observe that the lower scales capture the coarse motion trends, while higher scales provide a finer-grained depiction of the motion. For instance, the reconstruction result of “MSQ(1, 1)” reflects only the rough trajectory of the motion, neglecting the finer limb dynamics. In contrast, the result of “MSQ(1, 6)” closely matches the ground truth. These findings highlight the effectiveness of the multi-scale structure in our proposed representation, which potentially facilitates the flexibility in handling diverse motion modeling tasks.

Motion Composition and Control We qualitatively demonstrate the composition capability of our representation in Fig. 5. Our method enables the direct composition of two motion sequences

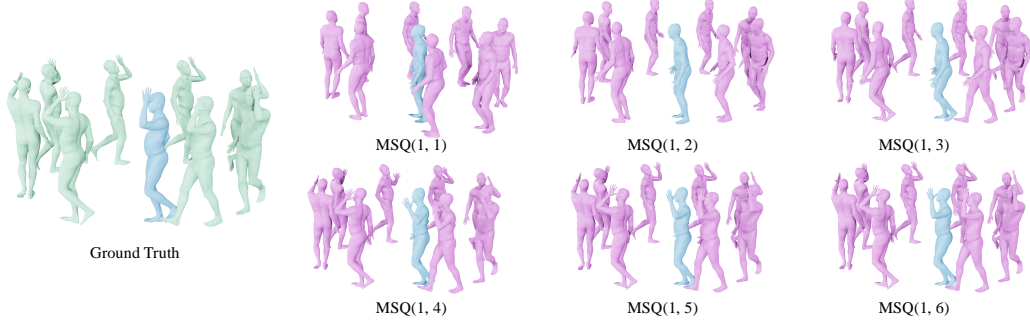


Figure 4: **Multi-scale visualization.** We present the reconstruction results of model “MSQ(1, s)”. The lower scales capture the coarse motion trends, while higher scales depict the motion in a finer granularity. The pose in blue denotes the first frame of each motion sequence.

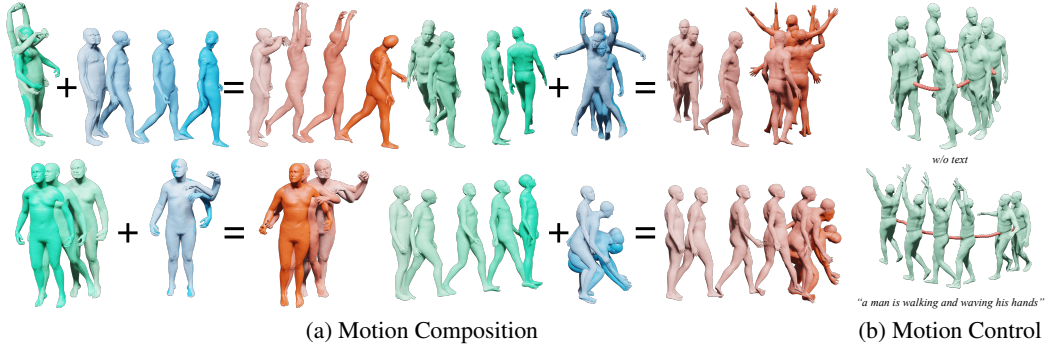


Figure 5: **Motion composition and control.** (a) Given two motion sequences, shown in green and blue, MSQ’s inherent capability enables the seamless composition of corresponding tokens for spatial (left two cases) and temporal (right two cases) motion composition. (b) Our method can also generate controllable motions aligning well with the given pelvis trajectory (red balls), with or without text conditions.

Table 2: **Quantitative results on the MotionFix [5].** “Real” denotes results computed from ground truth. **Bold** indicates the best result.

Model	Data	Source Input	generated-to-target retrieval				generated-to-source retrieval			
			R@1↑	R@2↑	R@3↑	AvgR↓	R@1↑	R@2↑	R@3↑	AvgR↓
Real	-	-	100.0	100.0	100.0	1.00	74.01	84.52	89.91	2.03
MDM	HumanML3D	✗	4.03	7.56	10.48	15.55	2.62	6.15	9.38	15.88
MDM _s	HumanML3D	✓	3.63	7.06	10.08	15.64	2.62	6.25	9.78	15.84
MDM-BP	HumanML3D	✗	39.10	50.09	54.84	6.46	61.28	69.55	73.99	4.21
MDM-BP _s	HumanML3D	✓	38.10	48.99	54.84	6.47	60.28	69.46	73.89	4.23
MDM [57]	MotionFix	✓	18.54	29.17	36.04	11.91	15.01	23.75	31.04	11.96
TMED [5]	MotionFix	✓	62.90	76.51	83.06	2.71	71.77	84.07	89.52	1.96
Ours	MotionFix	✓	68.18	82.62	87.64	2.30	74.50	87.22	91.17	1.92

along temporal or spatial dimensions, yielding plausible outcomes that capture partial dynamics from both motions, as shown in Fig. 5a. Additionally, this capability allows the decomposition of body parts at specific scales, such as capturing pelvis information in the first scale. We quantize the pelvis trajectory into discrete tokens and use them to control motion generation via a pre-trained masked transformer. Fig. 5b presents the generated results that closely align with the guided pelvis trajectory, regardless of whether using text conditions.

5.2 Evaluation on MotionFix

Setting, Metrics, and Baselines MotionFix [5] is a recently established text-based motion editing benchmark, requiring generation models to produce a plausible target human motion given a source motion and edited text prompt. It includes 6, 730 source-target motion pairs with text annotations for training and evaluation. We use MotionFix’s original raw pose representations and dataset splits. The evaluation adopts motion-to-motion retrieval metrics, including recall precision at rank k (i.e., $R@1$, $R@2$, $R@3$) and average ranking (i.e., $AvgR$), to assess how accurately the target (*generated-to-target*

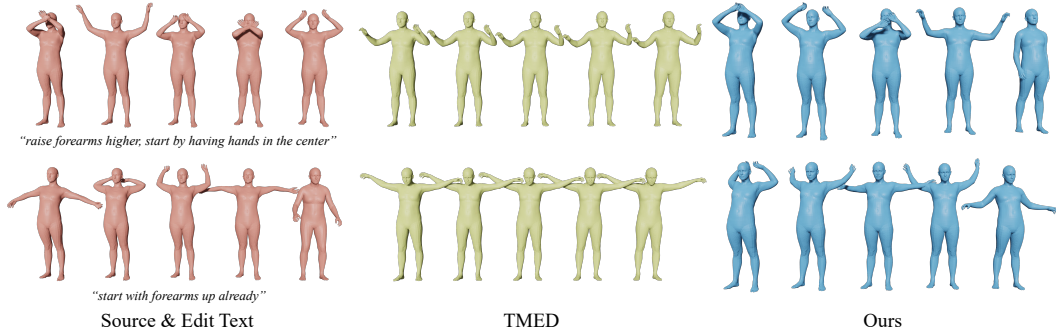


Figure 6: **Qualitative results on MotionFix dataset.** Given editing texts and source motions, our method successfully generates plausible target motions, while the state-of-the-art method TMED [5] fails to effectively align the edit parts with descriptions.

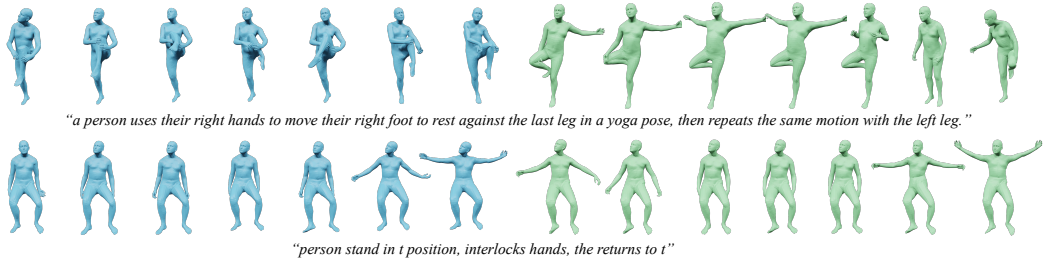


Figure 7: **Generation results on HumanML3D evaluation set.** MoMask [23] fails to generate complex composite motions like “perform one action first then follow with another”, whereas our results successfully capture the described dynamics.

retrieval) or source motion (*generated-to-source retrieval*) can be retrieved by the generated motion. We compare our method with baseline methods from Athanasiou et al. [5], including MDM, MDM_s, MDM-BP, MDM-BP_s, and TMED. The subscript _s indicates that the model initializes with the source motion instead of random noise for denoising. The “BD” label denotes that the model uses a large language model to identify body parts irrelevant to the edit text, keeping these parts fixed via masking.

Results As shown in Tab. 2, our method outperforms the baselines in both *generated-to-target retrieval* and *generated-to-source retrieval* precision. We emphasize that *generated-to-target retrieval* is the primary performance metric, as it reflects how closely the generated results align with the target. Our representation’s inherent multi-scale and compositional properties facilitate learning the relationship between body part dynamics and editing text, significantly improving the accuracy of editing results. Fig. 6 visually compares TMED [5] and our method, showing that our approach captures the edited parts more accurately than TMED, demonstrating its superior performance.

5.3 Evaluation on HumanML3D

Setting, Metrics, and Baselines We evaluate our method on one of the most popular text-to-motion benchmarks, *i.e.*, HumanML3D [22], which contains 14,616 motion sequences, each described by three text descriptions. In addition to standard metrics such as *FID*, *R-Precision*, *MM Dist.*, *Diversity*, and *MultiModality*, we report the *TMR Similarity Score (TMR)* by following Petrovich et al. [48] to evaluate text-motion similarity using contrastive learning-trained encoders, which are proven more effective in capturing complex text-motion relationships. We also compute a *Success Rate (Succ. Rate)*, considering a test case successful if its TMR similarity score exceeds a threshold of 0.7. We report the mean per joint position error (MPJPE) in millimeters when evaluating the reconstruction quality of MSQ. The comparison baselines include T2M [22], MDM [57], MLD [10], T2M-GPT [70], and MoMask [23], with which we adopt the same pose representation and dataset split.

Results We present the quantitative results in Tab. 3, where our model achieves the best FID, TMR, and Succ. Rate, demonstrating the effectiveness of our proposed methods. The discrepancy between R-Precision and Succ. Rate further suggests significant variance in these metrics when evaluating the consistency between generated motions and text descriptions, highlighting the limitations of these metrics. The qualitative results on the HumanML3D test set are shown in Fig. 7. MoMask [23]

Table 3: **Quantitative results of text-to-motion on the HumanML3D [22].** “Real” denotes results computed from ground truth. \pm indicates the 95% confidence interval based on twenty repeated evaluations. **Bold** indicates the best result. “†” denotes the reproduced results, which are slightly inconsistent with the paper-reported results (shown in gray color). The issue is discussed in <https://github.com/EricGuo5513/momask-codes/issues/27>.

Model	R-Precision (Top 1) \uparrow	FID \downarrow	MM Dist. \downarrow	MultiModality \uparrow	TMR \uparrow	Succ. Rate \uparrow
Real	0.511 \pm .003	0.002 \pm .000	2.974 \pm .008	-	0.530	0.305
T2M [22]	0.457 \pm .002	1.067 \pm .002	3.340 \pm .008	2.090 \pm .083	-	-
T2M-GPT [70]	0.491 \pm .003	0.116 \pm .004	3.118 \pm .011	1.865 \pm .011	-	-
MDM [57]	0.319 \pm .005	0.544 \pm .044	5.566 \pm .027	2.799\pm.072	0.378 \pm .005	0.079 \pm .003
MLD [10]	0.481 \pm .003	0.473 \pm .013	3.196 \pm .010	2.413 \pm .079	0.437 \pm .003	0.191 \pm .004
MoMask [†] [23]	0.504\pm.003	0.124 \pm .006	3.042\pm.010	1.313 \pm .044	0.503 \pm .006	0.285 \pm .004
MoMask [23]	0.521 \pm .002	0.045 \pm .002	2.958 \pm .008	1.241 \pm .040	0.531 \pm .005	0.289 \pm .002
Ours	0.483 \pm .005	0.063\pm.007	3.094 \pm .019	1.290 \pm .041	0.521\pm.003	0.297\pm.006

struggles to generate motions where the left and right legs move successively or where two consecutive T-poses are performed. In contrast, our method successfully generates plausible dynamics for such complex compositional descriptions.

5.4 Evaluation on HUMANISE

Setting, Metrics, and Baselines HUMANISE [61] introduces a more challenging conditional motion generation task, *i.e.*, language-guided human motion generation in 3D scenes, which necessitates a joint modeling of text, 3D scenes, and human motion. Our evaluation follows the setting from Wang et al. [62]. We report results using metrics: *goal dist.* for measuring the grounding accuracy of the target interactive object, along with *contact score* and *non-collision score* for evaluating the physical plausibility of the generated motion within 3D scenes. The baselines include all methods compared in Wang et al. [62]. Notably, Wang et al. [62] introduces a two-stage framework that leverages the scene affordance as an intermediary. We replace their second-stage model with our methods as our solution.

Results Tab. 4 presents the quantitative results. Our method outperforms all baselines regarding *goal dist.* and *non-collision* scores, indicating our representation’s effectiveness in the joint modeling of motion, text, and 3D scene. This effective modeling enhances the accuracy of grounding target interactive objects and improves scene awareness for collision-free motion generation.

Table 4: **Quantitative results of motion generation on the HUMANISE [61].** **Bold** indicates the best result. Each evaluation is repeated five times with a 95% confidence interval indicated by \pm .

Model	goal dist. \downarrow	contact \uparrow	non-collision \uparrow
cVAE [61]	0.422 \pm .011	84.06 \pm .716	99.77 \pm .004
one-stage@Enc [62]	0.326 \pm .013	76.11 \pm .684	99.71 \pm .014
one-stage@Dec [62]	0.185 \pm .014	86.43 \pm .845	99.76 \pm .006
two-stage@Enc [62]	0.156 \pm .006	95.86 \pm .323	99.69 \pm .007
two-stage@Dec [62]	0.156 \pm .006	96.04\pm.298	99.70 \pm .005
Ours	0.125\pm.004	93.10 \pm .180	99.78\pm.010

6 Conclusion

This paper targets flexible motion representation by proposing a novel quantization method, which compresses motion sequences into a multi-scale, compositional discrete token space. We highlight the inherent composition capability of this representation by directly composing tokens from different motion sequences. Additionally, we incorporate generative masked modeling to support diverse motion modeling tasks, including motion editing, control, and conditional generation, and demonstrate its superior performance across multiple benchmarks.

Limitations Our multi-scale quantization approach results in a larger number of tokens compared to typical frame-level quantization methods like T2M-GPT [70], making the second stage of transformer-based inference computationally intensive. Additionally, the manual definition of spatial scales may lead to suboptimal representations.

Acknowledgments This work is supported in part by the National Science and Technology Major Project (2022ZD0114900) and the National Natural Science Foundation of China (NSFC) (62172043).

References

- [1] Kfir Aberman, Yijia Weng, Dani Lischinski, Daniel Cohen-Or, and Baoquan Chen. Unpaired motion style transfer from video to animation. *ACM Transactions on Graphics (TOG)*, 39(4):64–1, 2020. 3
- [2] Nasir Ahmed, T. Natarajan, and Kamisetty R. Rao. Discrete cosine transform. *IEEE Transactions on Computers*, 100(1):90–93, 1974. 3
- [3] Chaitanya Ahuja and Louis-Philippe Morency. Language2pose: Natural language grounded pose forecasting. In *International Conference on 3D Vision (3DV)*, 2019. 2
- [4] Joao Pedro Araújo, Jiaman Li, Karthik Vetrivel, Rishi Agarwal, Jiajun Wu, Deepak Gopinath, Alexander William Clegg, and Karen Liu. Circle: Capture in rich contextual environments. In *Conference on Computer Vision and Pattern Recognition (CVPR)*, 2023. 3
- [5] Nikos Athanasiou, Alpár Ceske, Markos Diomataris, Michael J. Black, and Gül Varol. MotionFix: Text-driven 3d human motion editing. In *ACM SIGGRAPH Conference Proceedings*, 2024. 2, 3, 5, 7, 8, 18
- [6] Yoshua Bengio, Nicholas Léonard, and Aaron Courville. Estimating or propagating gradients through stochastic neurons for conditional computation. *arXiv preprint arXiv:1308.3432*, 2013. 3
- [7] Zhe Cao, Hang Gao, Karttikeya Mangalam, Qi-Zhi Cai, Minh Vo, and Jitendra Malik. Long-term human motion prediction with scene context. In *European Conference on Computer Vision (ECCV)*, 2020. 2, 3
- [8] Huiwen Chang, Han Zhang, Lu Jiang, Ce Liu, and William T Freeman. Maskgit: Masked generative image transformer. In *Conference on Computer Vision and Pattern Recognition (CVPR)*, 2022. 2, 3, 6
- [9] Huiwen Chang, Han Zhang, Jarred Barber, AJ Maschinot, Jose Lezama, Lu Jiang, Ming-Hsuan Yang, Kevin Murphy, William T Freeman, Michael Rubinstein, et al. Muse: Text-to-image generation via masked generative transformers. *arXiv preprint arXiv:2301.00704*, 2023. 3
- [10] Xin Chen, Biao Jiang, Wen Liu, Zilong Huang, Bin Fu, Tao Chen, and Gang Yu. Executing your commands via motion diffusion in latent space. In *Conference on Computer Vision and Pattern Recognition (CVPR)*, 2023. 2, 3, 8, 9, 15
- [11] Kiran Chhatre, Nikos Athanasiou, Giorgio Becherini, Christopher Peters, Michael J Black, Timo Bolkart, et al. Emotional speech-driven 3d body animation via disentangled latent diffusion. In *Conference on Computer Vision and Pattern Recognition (CVPR)*, 2024. 3
- [12] Jieming Cui, Tengyu Liu, Nian Liu, Yaodong Yang, Yixin Zhu, and Siyuan Huang. Anyskill: Learning open-vocabulary physical skill for interactive agents. In *Conference on Computer Vision and Pattern Recognition (CVPR)*, 2024. 3
- [13] Wenxun Dai, Ling-Hao Chen, Jingbo Wang, Jinpeng Liu, Bo Dai, and Yansong Tang. Motionlcm: Real-time controllable motion generation via latent consistency model. In *European Conference on Computer Vision (ECCV)*, 2024. 2, 3
- [14] Jacob Devlin. Bert: Pre-training of deep bidirectional transformers for language understanding. *arXiv preprint arXiv:1810.04805*, 2018. 3
- [15] Prafulla Dhariwal and Alexander Nichol. Diffusion models beat gans on image synthesis. In *Advances in Neural Information Processing Systems (NeurIPS)*, 2021. 3
- [16] Prafulla Dhariwal, Heewoo Jun, Christine Payne, Jong Wook Kim, Alec Radford, and Ilya Sutskever. Jukebox: A generative model for music. *arXiv preprint arXiv:2005.00341*, 2020. 3
- [17] Christian Diller and Angela Dai. Cg-hoi: Contact-guided 3d human-object interaction generation. In *Conference on Computer Vision and Pattern Recognition (CVPR)*, 2024. 2, 3
- [18] Patrick Esser, Robin Rombach, and Bjorn Ommer. Taming transformers for high-resolution image synthesis. In *Conference on Computer Vision and Pattern Recognition (CVPR)*, 2021. 3
- [19] Purvi Goel, Kuan-Chieh Wang, C Karen Liu, and Kayvon Fatahalian. Iterative motion editing with natural language. In *ACM SIGGRAPH Conference Proceedings*, 2024. 2, 3
- [20] Ian Goodfellow, Jean Pouget-Abadie, Mehdi Mirza, Bing Xu, David Warde-Farley, Sherjil Ozair, Aaron Courville, and Yoshua Bengio. Generative adversarial nets. In *Advances in Neural Information Processing Systems (NeurIPS)*, 2014. 3

- [21] Chuan Guo, Xinxin Zuo, Sen Wang, Shihao Zou, Qingyao Sun, Annan Deng, Minglun Gong, and Li Cheng. Action2motion: Conditioned generation of 3d human motions. In *International Conference on Multimedia*, 2020. 2
- [22] Chuan Guo, Shihao Zou, Xinxin Zuo, Sen Wang, Wei Ji, Xingyu Li, and Li Cheng. Generating diverse and natural 3d human motions from text. In *Conference on Computer Vision and Pattern Recognition (CVPR)*, 2022. 1, 2, 3, 6, 8, 9, 15, 17, 18
- [23] Chuan Guo, Yuxuan Mu, Muhammad Gohar Javed, Sen Wang, and Li Cheng. Momask: Generative masked modeling of 3d human motions. In *Conference on Computer Vision and Pattern Recognition (CVPR)*, 2024. 1, 2, 3, 6, 8, 9, 15
- [24] Jonathan Ho, Ajay Jain, and Pieter Abbeel. Denoising diffusion probabilistic models. In *Advances in Neural Information Processing Systems (NeurIPS)*, 2020. 3
- [25] Siyuan Huang, Zan Wang, Puhao Li, Baoxiong Jia, Tengyu Liu, Yixin Zhu, Wei Liang, and Song-Chun Zhu. Diffusion-based generation, optimization, and planning in 3d scenes. In *Conference on Computer Vision and Pattern Recognition (CVPR)*, 2023. 2, 3
- [26] Deok-Kyeong Jang, Soomin Park, and Sung-Hee Lee. Motion puzzle: Arbitrary motion style transfer by body part. *ACM Transactions on Graphics (TOG)*, 41(3):1–16, 2022. 3
- [27] Biao Jiang, Xin Chen, Wen Liu, Jingyi Yu, Gang Yu, and Tao Chen. Motiongpt: Human motion as a foreign language. In *Advances in Neural Information Processing Systems (NeurIPS)*, 2023. 3
- [28] Nan Jiang, Tengyu Liu, Zhexuan Cao, Jieming Cui, Zhiyuan Zhang, Yixin Chen, He Wang, Yixin Zhu, and Siyuan Huang. Full-body articulated human-object interaction. In *International Conference on Computer Vision (ICCV)*, 2023. 3
- [29] Nan Jiang, Zhiyuan Zhang, Hongjie Li, Xiaoxuan Ma, Zan Wang, Yixin Chen, Tengyu Liu, Yixin Zhu, and Siyuan Huang. Scaling up dynamic human-scene interaction modeling. In *Conference on Computer Vision and Pattern Recognition (CVPR)*, 2024. 1, 3
- [30] Tero Karras. Progressive growing of gans for improved quality, stability, and variation. In *International Conference on Learning Representations (ICLR)*, 2018. 2
- [31] Tero Karras, Samuli Laine, and Timo Aila. A style-based generator architecture for generative adversarial networks. In *Conference on Computer Vision and Pattern Recognition (CVPR)*, 2019. 3
- [32] Korrawe Karunratanakul, Konpat Preechakul, Supasorn Suwajanakorn, and Siyu Tang. Guided motion diffusion for controllable human motion synthesis. In *International Conference on Computer Vision (ICCV)*, 2023. 2, 3
- [33] Katsura. Cosine Annealing with Warmup for PyTorch. <https://github.com/katsura-jp/pytorch-cosine-annealing-with-warmup>, 2024. Accessed: 2024-11-15. 6
- [34] Diederik P Kingma. Auto-encoding variational bayes. *arXiv preprint arXiv:1312.6114*, 2013. 2
- [35] Doyup Lee, Chiheon Kim, Saehoon Kim, Minsu Cho, and Wook-Shin Han. Autoregressive image generation using residual quantization. In *Conference on Computer Vision and Pattern Recognition (CVPR)*, 2022. 5
- [36] Jiaman Li, Jiajun Wu, and C Karen Liu. Object motion guided human motion synthesis. *ACM Transactions on Graphics (TOG)*, 42(6):1–11, 2023. 1, 2, 3
- [37] Tianhong Li, Huiwen Chang, Shlok Mishra, Han Zhang, Dina Katabi, and Dilip Krishnan. MAGE: Masked generative encoder to unify representation learning and image synthesis. In *Conference on Computer Vision and Pattern Recognition (CVPR)*, 2023. 3
- [38] Han Liang, Wenqian Zhang, Wenxuan Li, Jingyi Yu, and Lan Xu. Intergen: Diffusion-based multi-human motion generation under complex interactions. *International Journal of Computer Vision (IJCV)*, pages 1–21, 2024. 3
- [39] Tsung-Yi Lin, Piotr Dollár, Ross Girshick, Kaiming He, Bharath Hariharan, and Serge Belongie. Feature pyramid networks for object detection. In *Conference on Computer Vision and Pattern Recognition (CVPR)*, 2017. 2
- [40] Matthew Loper, Naureen Mahmood, Javier Romero, Gerard Pons-Moll, and Michael J. Black. SMPL: A skinned multi-person linear model. *ACM Transactions on Graphics (TOG)*, 34(6):248:1–248:16, 2015. 2, 3

- [41] Shunlin Lu, Ling-Hao Chen, Ailing Zeng, Jing Lin, Ruimao Zhang, Lei Zhang, and Heung-Yeung Shum. Humantomato: Text-aligned whole-body motion generation. In *International Conference on Machine Learning (ICML)*, 2024. 2, 3
- [42] Wei Mao, Miaomiao Liu, and Mathieu Salzmann. History repeats itself: Human motion prediction via motion attention. In *European Conference on Computer Vision (ECCV)*, 2020. 2, 3
- [43] Fabian Mentzer, David Minnen, Eirikur Agustsson, and Michael Tschannen. Finite scalar quantization: Vq-vae made simple. In *International Conference on Learning Representations (ICLR)*, 2024. 2, 3, 4, 5
- [44] Georgios Pavlakos, Vasileios Choutas, Nima Ghorbani, Timo Bolkart, Ahmed AA Osman, Dimitrios Tzionas, and Michael J Black. Expressive body capture: 3d hands, face, and body from a single image. In *Conference on Computer Vision and Pattern Recognition (CVPR)*, 2019. 3
- [45] Xue Bin Peng, Ze Ma, Pieter Abbeel, Sergey Levine, and Angjoo Kanazawa. Amp: Adversarial motion priors for stylized physics-based character control. *ACM Transactions on Graphics (TOG)*, 40(4):1–20, 2021. 3
- [46] Mathis Petrovich, Michael J Black, and Gül Varol. Action-conditioned 3d human motion synthesis with transformer vae. In *International Conference on Computer Vision (ICCV)*, 2021. 1, 2, 3
- [47] Mathis Petrovich, Michael J Black, and Gül Varol. Temos: Generating diverse human motions from textual descriptions. In *European Conference on Computer Vision (ECCV)*, 2022. 1, 2, 3
- [48] Mathis Petrovich, Michael J Black, and Gül Varol. Tmr: Text-to-motion retrieval using contrastive 3d human motion synthesis. In *International Conference on Computer Vision (ICCV)*, 2023. 8
- [49] Huaijin Pi, Sida Peng, Minghui Yang, Xiaowei Zhou, and Hujun Bao. Hierarchical generation of human-object interactions with diffusion probabilistic models. In *International Conference on Computer Vision (ICCV)*, 2023. 2, 3, 4, 14
- [50] Ekkasit Pinyoanuntapong, Pu Wang, Minwoo Lee, and Chen Chen. MMM: Generative masked motion model. In *Conference on Computer Vision and Pattern Recognition (CVPR)*, 2024. 2, 3
- [51] Alec Radford, Jong Wook Kim, Chris Hallacy, Aditya Ramesh, Gabriel Goh, Sandhini Agarwal, Girish Sastry, Amanda Askell, Pamela Mishkin, Jack Clark, et al. Learning transferable visual models from natural language supervision. In *International Conference on Machine Learning (ICML)*, 2021. 5, 16
- [52] Davis Rempe, Tolga Birdal, Aaron Hertzmann, Jimei Yang, Srinath Sridhar, and Leonidas J Guibas. Humor: 3d human motion model for robust pose estimation. In *International Conference on Computer Vision (ICCV)*, 2021. 3
- [53] Davis Rempe, Zhengyi Luo, Xue Bin Peng, Ye Yuan, Kris Kitani, Karsten Kreis, Sanja Fidler, and Or Litany. Trace and pace: Controllable pedestrian animation via guided trajectory diffusion. In *Conference on Computer Vision and Pattern Recognition (CVPR)*, 2023. 2, 3
- [54] Robin Rombach, Andreas Blattmann, Dominik Lorenz, Patrick Esser, and Björn Ommer. High-resolution image synthesis with latent diffusion models. In *Conference on Computer Vision and Pattern Recognition (CVPR)*, 2022. 3
- [55] Wenfeng Song, Xingliang Jin, Shuai Li, Chenglizhao Chen, Aimin Hao, Xia Hou, Ning Li, and Hong Qin. Arbitrary motion style transfer with multi-condition motion latent diffusion model. In *Conference on Computer Vision and Pattern Recognition (CVPR)*, 2024. 3
- [56] Haowen Sun, Ruikun Zheng, Haibin Huang, Chongyang Ma, Hui Huang, and Ruizhen Hu. Lgtm: Local-to-global text-driven human motion diffusion model. In *ACM SIGGRAPH Conference Proceedings*, 2024. 3
- [57] Guy Tevet, Sigal Raab, Brian Gordon, Yoni Shafir, Daniel Cohen-or, and Amit Haim Bermano. Human motion diffusion model. In *International Conference on Learning Representations (ICLR)*, 2023. 1, 2, 3, 7, 8, 9, 15
- [58] Keyu Tian, Yi Jiang, Zehuan Yuan, Bingyue Peng, and Liwei Wang. Visual autoregressive modeling: Scalable image generation via next-scale prediction. In *Advances in Neural Information Processing Systems (NeurIPS)*, 2024. 2, 3
- [59] Aaron Van Den Oord, Oriol Vinyals, et al. Neural discrete representation learning. In *Advances in Neural Information Processing Systems (NeurIPS)*, 2017. 2, 3

- [60] Weilin Wan, Zhiyang Dou, Taku Komura, Wenping Wang, Dinesh Jayaraman, and Lingjie Liu. Tlcontrol: Trajectory and language control for human motion synthesis. In *European Conference on Computer Vision (ECCV)*, 2024. 2, 3, 4, 14
- [61] Zan Wang, Yixin Chen, Tengyu Liu, Yixin Zhu, Wei Liang, and Siyuan Huang. Humanise: Language-conditioned human motion generation in 3d scenes. In *Advances in Neural Information Processing Systems (NeurIPS)*, 2022. 2, 3, 9, 17, 18
- [62] Zan Wang, Yixin Chen, Baoxiong Jia, Puhao Li, Jinlu Zhang, Jingze Zhang, Tengyu Liu, Yixin Zhu, Wei Liang, and Siyuan Huang. Move as you say, interact as you can: Language-guided human motion generation with scene affordance. In *Conference on Computer Vision and Pattern Recognition (CVPR)*, 2024. 3, 9, 16, 18
- [63] Zeqi Xiao, Tai Wang, Jingbo Wang, Jinkun Cao, Wenwei Zhang, Bo Dai, Dahua Lin, and Jiangmiao Pang. Unified human-scene interaction via prompted chain-of-contacts. In *International Conference on Learning Representations (ICLR)*, 2024. 3
- [64] Yiming Xie, Varun Jampani, Lei Zhong, Deqing Sun, and Huaizu Jiang. Omnicontrol: Control any joint at any time for human motion generation. In *International Conference on Learning Representations (ICLR)*, 2024. 2, 3
- [65] Liang Xu, Xintao Lv, Yichao Yan, Xin Jin, Shuwen Wu, Congsheng Xu, Yifan Liu, Yizhou Zhou, Fengyun Rao, Xingdong Sheng, et al. Inter-x: Towards versatile human-human interaction analysis. In *Conference on Computer Vision and Pattern Recognition (CVPR)*, 2024. 3
- [66] Hongwei Yi, Justus Thies, Michael J Black, Xue Bin Peng, and Davis Rempe. Generating human interaction motions in scenes with text control. In *European Conference on Computer Vision (ECCV)*, 2024. 3
- [67] Jiahui Yu, Yuanzhong Xu, Jing Yu Koh, Thang Luong, Gunjan Baid, Zirui Wang, Vijay Vasudevan, Alexander Ku, Yinfei Yang, Burcu Karagol Ayan, et al. Scaling autoregressive models for content-rich text-to-image generation. *arXiv preprint arXiv:2206.10789*, 2022. 3
- [68] Ye Yuan and Kris Kitani. Dlow: Diversifying latent flows for diverse human motion prediction. In *European Conference on Computer Vision (ECCV)*, 2020. 2, 3
- [69] Canyu Zhang, Youbao Tang, Ning Zhang, Ruei-Sung Lin, Mei Han, Jing Xiao, and Song Wang. Bidirectional autoregressive diffusion model for dance generation. In *Conference on Computer Vision and Pattern Recognition (CVPR)*, 2024. 3
- [70] Jianrong Zhang, Yangsong Zhang, Xiaodong Cun, Shaoli Huang, Yong Zhang, Hongwei Zhao, Hongtao Lu, and Xi Shen. T2M-GPT: Generating human motion from textual descriptions with discrete representations. In *Conference on Computer Vision and Pattern Recognition (CVPR)*, 2023. 1, 2, 3, 8, 9, 15
- [71] Mingyuan Zhang, Xinying Guo, Liang Pan, Zhongang Cai, Fangzhou Hong, Huirong Li, Lei Yang, and Ziwei Liu. Remodiffuse: Retrieval-augmented motion diffusion model. In *International Conference on Computer Vision (ICCV)*, 2023. 2
- [72] Mingyuan Zhang, Huirong Li, Zhongang Cai, Jiawei Ren, Lei Yang, and Ziwei Liu. Finemogen: Fine-grained spatio-temporal motion generation and editing. In *Advances in Neural Information Processing Systems (NeurIPS)*, 2023. 1, 3
- [73] Siwei Zhang, Yan Zhang, Federica Bogo, Marc Pollefeys, and Siyu Tang. Learning motion priors for 4d human body capture in 3d scenes. In *International Conference on Computer Vision (ICCV)*, 2021. 3
- [74] Xiaohan Zhang, Bharat Lal Bhatnagar, Sebastian Starke, Vladimir Guzov, and Gerard Pons-Moll. Couch: Towards controllable human-chair interactions. In *European Conference on Computer Vision (ECCV)*, 2022. 3
- [75] Yan Zhang, Michael J Black, and Siyu Tang. We are more than our joints: Predicting how 3d bodies move. In *Conference on Computer Vision and Pattern Recognition (CVPR)*, 2021. 3
- [76] Chongyang Zhong, Lei Hu, Zihao Zhang, and Shihong Xia. Att2m: Text-driven human motion generation with multi-perspective attention mechanism. In *International Conference on Computer Vision (ICCV)*, 2023. 2, 3

Appendix

A MSQ Algorithm

We present the encoding and decoding algorithm of MSQ in Alg. 1. Here, $\text{Inter}(\mathbf{z}, n_s)$ denotes the interpolation operation that interpolates $\mathbf{z} \in \mathbb{R}^{n \times d}$ to $\bar{\mathbf{z}}_s \in \mathbb{R}^{n_s \times d}$, $\text{Concat}(\cdot)$ represents the concatenation operation, and $\text{FSQ-lookup}(\mathbf{y}_s)$ dequantizes the token indices \mathbf{y}_s into codes $\hat{\mathbf{z}}_s$.

Algorithm 1: Encoding and Decoding of MSQ

```

1 // Encoding Process
  Input: Raw motion sequence  $\mathbf{x}$ ;
2 Encoders  $\{\mathcal{E}_s\}_{s=1}^S, f_0 = \mathbf{0}, \mathbf{y} = []$ ;
3 Decompose  $\mathbf{x}$  into  $\{\bar{\mathbf{x}}_s\}_{s=1}^S$ ;
4 for  $s = 1, \dots, S$  do
5    $\mathbf{z}_s = \mathcal{E}_s(\bar{\mathbf{x}}_s)$ ;
6    $\bar{\mathbf{z}}_s = \text{Inter}(\mathbf{z}_s - f_{s-1}, n_s)$ ;
7    $\tilde{\mathbf{z}}_s, \mathbf{y}_s = \text{FSQ}(\bar{\mathbf{z}}_s)$ ;
8    $\mathbf{y} = \text{Concat}(\mathbf{y}, \mathbf{y}_s)$ ; // Concatenation
9    $\hat{\mathbf{z}}_s = \text{Inter}(\tilde{\mathbf{z}}_s, n)$ ;
10   $f_s = \sum_{i=1}^s \hat{\mathbf{z}}_i$ ;
  Output:  $\mathbf{y}$ ;
11 // Decoding Process
  Input: Motion token sequence  $\mathbf{y}$ ;
12 Decoder  $\mathcal{D}, \hat{f} = \mathbf{0}$ ;
13 Decompose  $\mathbf{y}$  into  $\{\mathbf{y}_s\}_{s=1}^S$ ;
14 for  $s = 1, \dots, S$  do
15    $\tilde{\mathbf{z}}_s = \text{FSQ-lookup}(\mathbf{y}_s)$ ; // Dequantization
16    $\hat{\mathbf{z}}_s = \text{Inter}(\tilde{\mathbf{z}}_s, n)$ ;
17    $\hat{f} = \hat{f} + \hat{\mathbf{z}}_s$ ;
18  $\hat{\mathbf{x}} = \mathcal{D}(\hat{f})$ ;
  Output:  $\hat{\mathbf{x}}$ ;

```

B Implementation Details

B.1 MSQ

Each scale feature represents a different level of spatial granularity in the motion sequence. Specifically, we decompose the raw motion \mathbf{x} into $\{\bar{\mathbf{x}}_s\}_{s=1}^S$ based on body parts by following prior works [49, 60], with each $\bar{\mathbf{x}}_s$ capturing distinct features associated with specific body parts. For all scales, Tab. A1 defines the body parts they encompass. Besides, each scale’s latent feature $\mathbf{z}_s \in \mathbb{R}^{n \times d}$ will be interpolated into $\bar{\mathbf{z}}_s \in \mathbb{R}^{n_s \times d}$ along the temporal dimension to construct the multi-scale structure. Tab. A1 also specifies the value of n_s for each scale. **Notably, we empirically define the scale for capturing specific body parts and the values of n_s for temporal interpolation. Alternative definitions are feasible but may slightly affect the final performance.** Each scale possesses a distinct quantizer in our implementation, thus resulting in varying quantization spaces across scales. By default, our implementation uses 6 scales. Tab. A1 also provides the configurations for the ablative models with varying numbers of scales used in the ablation study presented below. The model with 8 scales extends the default configuration by repeating the last scale twice.

B.2 Masked Transformer

Once the motion x is quantized into discrete index $\mathbf{y} = \{\mathbf{y}_s\}_{s=1}^S$, we flatten \mathbf{y} to form a token index sequence. For simplicity, we reuse \mathbf{y} to denote this flattened index sequence and assume its length is n . During the training of the masked transformer, we first randomly mask $\lceil \gamma(\tau) \cdot n \rceil$ tokens according to the masking schedule function $\gamma(\tau) = \cos(\frac{\pi\tau}{2})$, and replace them with [MASK] token. Here, $\tau \in [0, 1)$ is uniformly sampled from 0 to 1, and $\tau = 0$ means all tokens are masked. Then, the

Table A1: The detailed definition of each scale in MSQ.

Model	Scale	Body Part					n_s
		Pelvis	Torso	Legs	Arms	Head	
Two Scales	1	✓					16
	2	✓	✓	✓	✓	✓	49
Four Scales	1	✓	✓				16
	2	✓	✓	✓			24
	3	✓	✓	✓	✓		32
	4	✓	✓	✓	✓	✓	49
Six Scales (default)	1	✓					16
	2	✓	✓				24
	3	✓	✓	✓			32
	4	✓	✓	✓	✓		40
	5	✓	✓	✓	✓	✓	49
	6	✓	✓	✓	✓	✓	49

Table A2: Quantitative results of text-to-motion on the HumanML3D [22]. “Real” denotes results computed from ground truth. “→” indicates metrics are better when closer to the “Real”. ± indicates the 95% confidence interval based on twenty repeated evaluations.

Model	R-Precision ↑			FID ↓	MM Dist. ↓	Diversity →	MultiModality ↑	TMR ↑	Succ. Rate ↑
	Top 1	Top 2	Top 3						
Real	0.511±.003	0.703±.003	0.797±.002	0.002±.000	2.974±.008	9.503±.065	-	0.530	0.305
T2M [22]	0.457±.002	0.639±.003	0.740±.003	1.067±.002	3.340±.008	9.188±.002	2.090±.083	-	-
T2M-GPT [70]	0.491±.003	0.680±.003	0.775±.002	0.116±.004	3.118±.011	9.761±.081	1.865±.011	-	-
MDM [57]	0.319±.005	0.498±.004	0.611±.007	0.544±.044	5.566±.027	9.559±.086	2.799±.072	0.378±.005	0.079±.003
MLD [10]	0.481±.003	0.673±.003	0.772±.002	0.473±.013	3.196±.010	9.724±.082	2.413±.079	0.437±.003	0.191±.004
MoMask (Base) [†] [23]	0.503±.002	0.693±.002	0.791±.002	0.137±.006	3.056±.006	9.689±.089	1.102±.040	0.529±.004	0.289±.003
MoMask (Base) [23]	0.504±.004	0.699±.006	0.797±.004	0.082±.008	3.050±.013	-	1.050±.061	0.527±.003	0.283±.002
MoMask (Full) [†] [23]	0.504±.003	0.697±.002	0.795±.003	0.124±.006	3.042±.010	9.302±.077	1.313±.044	0.503±.006	0.285±.004
MoMask (Full) [23]	0.521±.002	0.713±.003	0.807±.002	0.045±.002	2.958±.008	9.624±.080	1.241±.040	0.531±.005	0.289±.002
Ours	0.483±.005	0.683±.002	0.778±.002	0.063±.007	3.094±.019	9.497±.204	1.290±.041	0.521±.003	0.297±.006

masked transformer learns to reconstruct the masked tokens by minimizing the following negative log-likelihood:

$$\mathcal{L} = \sum_{\tilde{\mathbf{y}}_i = [\text{MASK}]} -\log p_{\theta}(\mathbf{y}_i | \tilde{\mathbf{y}}, \mathcal{C}) \quad (\text{A1})$$

Here, $\tilde{\mathbf{y}}$ is the sequence after masking, i is the entry index, θ is model parameters, and \mathcal{C} is the input condition (*e.g.*, text). During the inference, the masked transformer starts with a fully masked token sequence and generates all tokens auto-regressively, as described in the main paper.

The model architecture builds on the implementation by Zhang et al. [70], while the masked modeling framework adopts the code from Guo et al. [23]. **We will release our code for reproducibility.**

B.3 Evaluation Details

For the evaluation on the MotionFix, HumanML3D, and HUMANISE benchmarks, we train our model from scratch using the corresponding benchmark-provided data, without any pretraining on other datasets. Below, we outline specific evaluation details for each benchmark.

Evaluation Details on MotionFix To train our masked transformer on MotionFix, we use the source motion token sequence as input, allowing the model to recover the target token sequence in a single iteration (*i.e.*, $K = 1$). Optionally, partial source motion tokens corresponding to the edited regions can be masked by leveraging ChatGPT to parse the editing text description. In our implementation, we use the original source motion tokens, which have already achieved promising results. Since MotionFix has not provided implementation details on using HumanML3D as a training data source, we did not evaluate our model leveraging HumanML3D data for training.

Evaluation Details on HumanML3D The standard evaluation metrics include (1) *FID*, measuring the distributional discrepancy between generated and real motions; (2) *R-Precision* and *MM Dist.*, assessing the relevance between the generated results and descriptions; (3) *Diversity*, evaluating the overall variation of all results; (4) *MultiModality*, evaluating the average variation of motions generated from one text. To compute these metrics, we follow prior works by sampling a single

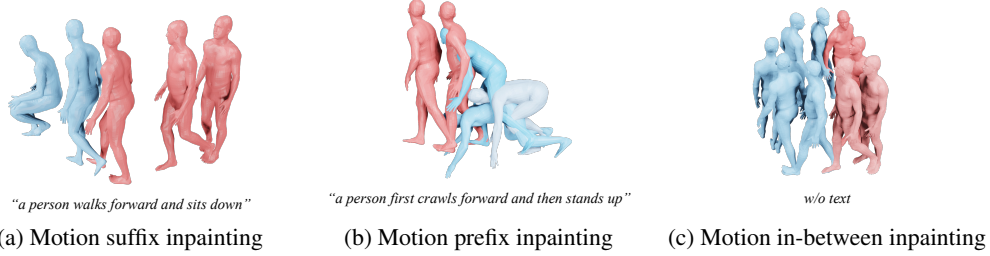


Figure A1: **Temporal motion inpainting**. Poses in **red** denotes the given frames, and poses in **blue** are recovered frames.

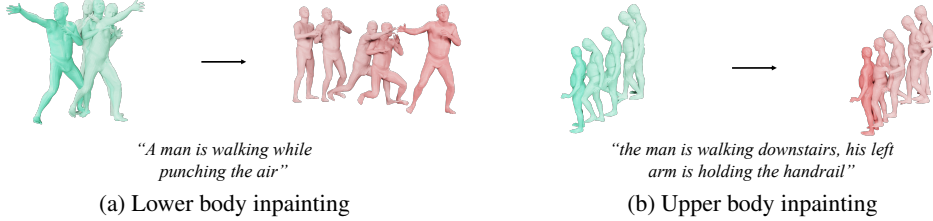


Figure A2: **Spatial motion inpainting**. Motions in **green** are the source motions, and motions in **red** are the inpainting results.

Table A3: **Quantitative results on five motion inpainting tasks.**

Task	R-Precision (Top 1) \uparrow	FID \downarrow	MM Dist. \downarrow	Diversity \rightarrow
In-betweening	$0.496 \pm .003$	$0.067 \pm .002$	$3.004 \pm .007$	$9.331 \pm .087$
Suffix Inpainting	$0.498 \pm .003$	$0.107 \pm .002$	$3.004 \pm .007$	$9.264 \pm .066$
Prefix Inpainting	$0.506 \pm .003$	$0.062 \pm .002$	$2.978 \pm .008$	$9.416 \pm .084$
Upper Body Editing	$0.499 \pm .004$	$0.115 \pm .003$	$3.032 \pm .009$	$9.432 \pm .097$
Lower Body Editing	$0.473 \pm .003$	$0.210 \pm .004$	$3.138 \pm .007$	$9.219 \pm .077$

description for each test case (each case in HumanML3D has three descriptions) during inference. Additionally, we introduce the TMR success rate to assess the correspondence between text and generated motion, but using all text descriptions for each test case during inference. Before computing the TMR score, we exclude low-quality descriptions where the TMR score computed with the ground-truth motion is below 0.3 to ensure evaluation quality. We use CLIP [51] to encode the text.

Evaluation Details on HUMANISE For evaluation on HUMANISE, we follow the setting in Wang et al. [62], and our method adapts their two-stage model for language-guided human motion generation in 3D scenes. Specifically, Wang et al. [62] proposes a two-stage framework that leverages scene affordance as an intermediary. We retain the first stage for affordance generation and replace the second-stage model with our masked transformer. We use the same encoder to process the affordance maps and the text descriptions, concatenate the resulting conditional tokens with the masked motion tokens, and pass the concatenation to the masked transformer, which only employs the self-attention mechanism in the design.

C Additional Results

The following text presents additional results of our method. **We recommend referring to the supplementary video for dynamic motion animations.**

C.1 Full Quantitative Results on HumanML3D

Tab. A2 presents the full quantitative result on HumanML3D. This table also reports the “MoMask (base)” model, which removes the residual transformer. “MoMask (full)” model includes these residual transformers for generating residual motion tokens. \dagger denotes the reproduced results, and the results in gray are original paper reported results.



Figure A3: Visualization results on HUMANISE.

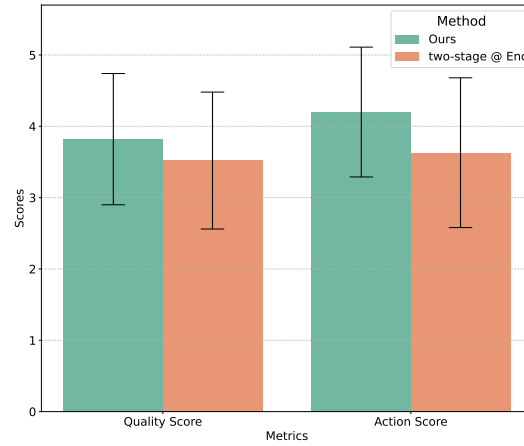


Figure A4: User study on HUMANISE.

C.2 Motion Inpainting Results

Our method supports both temporal and spatial inpainting of the motion sequence, and we evaluate the inpainting capability of our method across five tasks: motion in-betweening, suffix inpainting, prefix inpainting, upper body inpainting, and lower body inpainting. Specifically, during testing, we replace the partial frames or body part features with zero vectors, quantize the incomplete sequences using MSQ, and apply the pre-trained bidirectional masked transformer for recovery. For temporal inpainting, we mask 70% of the frames in the middle of the motion sequence for motion in-betweening, 70% of the frames at the beginning for motion prefix inpainting, and 70% of the frames at the end for suffix inpainting. For spatial inpainting, we mask the joint features of the upper or lower body for upper and lower body inpainting tasks. The motion inpainting results on HumanML3D [22], presented in Fig. A1, Fig. A2, and Tab. A3, highlight the effectiveness of our method in recovering incomplete motions.

C.3 Additional Results on HUMANISE

Visualization Results We present the visualization results of our method on the HUMANISE dataset in Fig. A3. These results demonstrate that our method effectively grounds target objects and generates physically plausible motion in 3D scenes guided by language descriptions.

User Study We further evaluate the generation quality through user study. Following HUMANISE [61], we ask users to rate the generated motions on a scale from 1 to 5 based on (i) overall generation quality (*i.e.*, *quality score*) and (ii) whether the motions accurately perform the action described by the text (*i.e.*, *action score*). Specifically, we generate 60 human-scene interaction cases

Table A4: Ablation of scale number S .

Model	R-Precision (Top 1) \uparrow	FID \downarrow	MM Dist. \downarrow	MPJPE \downarrow
Two Scales	$0.501 \pm .004$	$0.109 \pm .002$	$2.980 \pm .014$	$37.68 \pm .147$
Four Scales	$0.509 \pm .005$	$0.062 \pm .001$	$2.925 \pm .001$	$26.49 \pm .055$
Six Scales	$0.511 \pm .000$	$0.037 \pm .000$	$2.934 \pm .012$	$23.67 \pm .050$
Eight Scales	$0.513 \pm .004$	$0.018 \pm .000$	$2.912 \pm .012$	$16.41 \pm .030$

using the previous model, “two-stage @ Enc” proposed by Wang et al. [62], and another 60 cases using our method. These 120 cases are randomly shuffled and presented to four users. We report the results in Fig. A4, indicating that our method outperforms the previous approach in both *quality score* and *action score*.

C.4 Ablation Studies

We conduct ablation studies to investigate the impact of the scale number S . Tab. A4 presents the quantitative results. As S increases, MSQ demonstrates improved reconstruction quality, as metrics like *FID* and *MPJPE* indicate. However, *R-Precision* and *MM Dist.* begin to saturate when the scale number reaches 4, primarily because these metrics evaluate the alignment between motion and text in the high-level latent space, neglecting fine-grained details.

D Licenses for Existing Assets

We conduct our experiments on the MotionFix [5], HumanML3D [22], and HUMANISE [61] datasets. MotionFix is released under the terms of the [Creative Commons Attribution 4.0 International License](#), while both HumanML3D and HUMANISE are licensed under the [MIT License](#).

E Broader Impacts

This work on human motion generation holds the potential to positively impact a range of domains, including virtual reality (VR), assistive robotics, animation, and human-computer interaction. For instance, more realistic and controllable motion generation can enable more immersive and responsive virtual agents in education, training, or mental health applications. However, if misused, motion generation technologies may contribute to unethical surveillance systems or the creation of synthetic media that impersonate individuals without their consent.